

Scanning and Impedance Properties of TEM Horn Arrays for Transient Radiation

Daniel T. McGrath, *Member, IEEE*, and Carl E. Baum, *Fellow, IEEE*

Abstract—A general concept for ultrawide-band array design using interconnected transverse electromagnetic (TEM) horns is described. At high frequencies (wavelength small compared to unit cell dimensions), the mutual coupling between elements is small and, consequently, the input impedance depends only on the lattice dimensions and not on either scan angle or frequency. At low frequencies (wavelength large compared to unit cell dimensions), the mutual coupling is *purposefully* made large, by interconnecting the elements to maximize the low-frequency performance. This paper presents the results of analyses using a periodic hybrid finite-element approach to calculate input impedance and scanning performance of generic TEM horn arrays. The limiting case, the planar bicone, is shown to have the frequency-independent property of a self-complementary antenna, making it a useful case for establishing the effects of feed region geometry. Although it radiates bidirectionally, it has the interesting property that its broadside-scan frequency response in the array environment is absolutely flat up to the grating lobe onset limit. A TEM horn array is more unidirectional, but as a consequence suffers both oscillatory variations in the input impedance with frequency and increased limits on minimum achievable rise time.

Index Terms—Antenna arrays, horn antennas, transient radiation.

I. INTRODUCTION

A variety of interesting applications require the focused radiation of high-power transients. Some examples are electromagnetic pulse (EMP) simulators [1] and impulse radar such as that proposed for locating and identifying buried objects [2]. Requirements for these antennas include the need to radiate low-frequency components; in the former to reproduce a specific waveform and in the latter to be able to excite resonances of the objects of interest.

Although impulse radiating antennas using single sources with transverse electromagnetic (TEM) horns and reflectors have been successfully developed [1], [3], arrays would have several noteworthy advantages. For example, in an EMP simulator, an array of low-voltage pulsers triggered simultaneously would allow higher field strengths while preserving fast rise times [1], [4]. For an impulse radar, a single high-power switch source is undesirable because those available employ spark gaps that suffer pulse-to-pulse variations in the time the switch breaks relative to the triggering pulse (*jitter*). An array of low to medium power sources such as laser-triggered Gallium Arsenide switches, which do not suffer from jitter, would permit integration of pulses to achieve higher range resolution

Manuscript received May 12, 1997; revised June 11, 1998. This work was supported in part by the Air Force Office of Scientific Research.

The authors are with the Air Force Research Laboratory, Directed Energy Directorate, Kirtland AFB, NM 87117 USA.

Publisher Item Identifier S 0018-926X(99)04442-7.

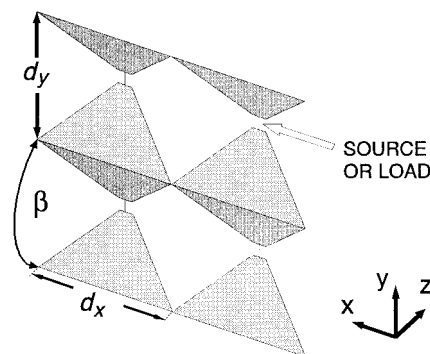


Fig. 1. TEM horn-array geometry.

[5]. Finally, an obvious advantage of a transient array would be the capability for electronic scanning by time delay.

A general concept for ultrawide-band array design using interconnected TEM horns (as illustrated in Fig. 1) has long been available [6]. Its asymptotic behavior at low and high frequencies is readily established. At high frequencies (wavelength small compared to unit cell dimensions) the mutual coupling between elements is small. At low frequencies (wavelength large compared to unit cell dimensions) the mutual coupling is *purposefully* large to maximize the low-frequency performance. However, little was known about the effects of mutual coupling at intermediate frequencies. This paper presents the results of analyses using a periodic hybrid finite-element approach, to calculate the input impedance and scanning performance of generic TEM horn arrays. These results confirm the asymptotic limits and, in addition, show that the arrays are capable of efficient radiation and reception over bandwidths limited on the upper end by grating lobe conditions, and on the lower end by the half-wavelength size of the entire array. In addition, tradeoffs between stability of input impedance with frequency and dispersion versus element directionality are illustrated.

II. ANALYSIS APPROACH

The analysis of mutual coupling effects begins with an assumption that the array is large enough that edge effects do not appreciably change the performance characteristics of the individual radiating elements. When that is the case, an infinite array assumption may be used to restrict the analysis to a single array unit cell. An important note is that a finite array does not radiate or receive efficiently at frequencies below that at which the entire array is a half wavelength in the direction of polarization. The computational method does not account for this low-frequency behavior or for edge effects in finite arrays.

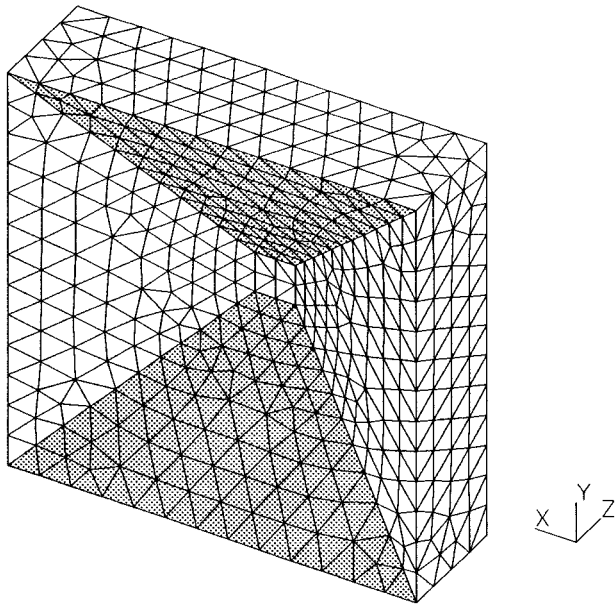


Fig. 2. Typical finite-element representation of array unit cell (mesh cells in horn interior removed).

In the periodic hybrid finite-element approach, presented in [7] and [8], the unit cell is subdivided into volume elements (tetrahedra) over which expansion functions for the electric field are defined. Fig. 2 shows an example “mesh” for a TEM horn element, with the cells in the horn interior blanked to show the shape of the conductors (shaded). The model may include resistive wires to emulate point sources or loads.

In this work, the field expansion functions are linear edge-based vector elements. The finite-element region is terminated at planes on the $+z$ and $-z$ sides of the structure, where a periodic radiation boundary condition is imposed. That condition, based on an integral equation, provides a reflectionless absorbing boundary for outgoing waves at all angles. In addition, periodicity conditions are enforced at the unit cell side walls, effectively wrapping opposing faces in x and y onto each other with a phase shift appropriate to the array scan angle. The formulation leads to a system of equations that must be constructed and solved separately for each scan angle and frequency.

In all of the cases discussed below, the mesh edge length was equal to or smaller than $\lambda/10$ at the highest frequency for which calculations were required and still finer in the vicinity of the feed points. The matrix solver used the biconjugate gradient method [9] with a residual error threshold of 1×10^{-5} . All Floquet modes of order $-10 \leq m \leq 10$ and $-10 \leq n \leq 10$ were used in calculating the matrix terms associated with the periodic radiation boundaries. These mesh granularities, mode limits, and residual thresholds were confirmed to give convergence of the calculated currents to within 0.1% [10].

III. PLANAR BICONE ARRAYS

A limiting case of the TEM horn, in which $\beta = 180^\circ$, is the “planar bicone.” A planar bicone array, illustrated in Fig. 3, is capable of radiating waveforms with very low-

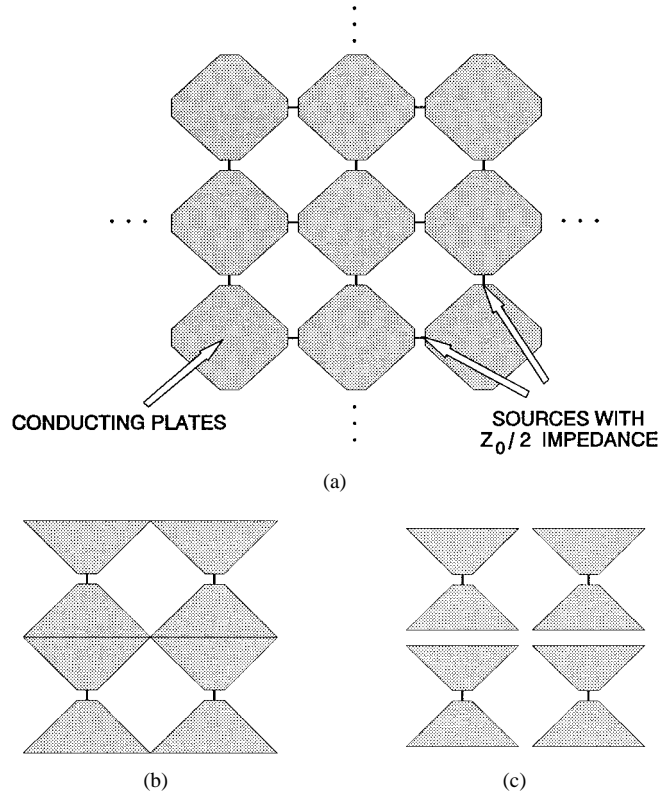


Fig. 3. Planar bicone-array geometry. (a) Dual polarized. (b) Vertically polarized. (c) Vertically polarized with gaps.

frequency components because the sources are connected in series. In practice, the low-frequency radiation will be limited by that frequency at which the entire (finite) array is one half wavelength across.

A planar bicone array is not optimal for most applications because it is bidirectional, radiating equally into each half-space at all frequencies. However, it is an interesting starting point for analysis because of the fact that when the lattice is square ($d_x = d_y$) it is “self-complementary.” That is, a rotation of 90° about any feed point results in the complementary structure with conductor replacing free-space and vice versa. Consequently, its input impedance must equal $\eta_0/2$, independent of frequency [11], where $\eta_0 = 120\pi \Omega$. This property has been confirmed for frequencies up to the half-wavelength lattice dimensions by measurements of a line-source array in parallel-plate waveguide [12]. The importance of studying the planar bicone array is that it allows an assessment of the effects of nonideal feed geometries. Fig. 4 shows two configurations, with Fig. 4(b) intended to better represent an ideal point source.

Computed values of Z_{in} for both feeds are shown in Fig. 5. Note that f_0 is that frequency at which the lattice dimensions are exactly one wavelength, i.e., $d_x = d_y = \lambda_0$. When frequency increases through f_0 , eight grating lobes enter visible space, four in each half-space causing an abrupt discontinuity in Z_{in} . When the frequency increases through $\sqrt{2}f_0$, a second set of grating lobes becomes visible causing another discontinuity. In spite of those grating lobes, the input impedance remains near the expected value of $60\pi \Omega$, confirming its self-complementary property. As expected, the

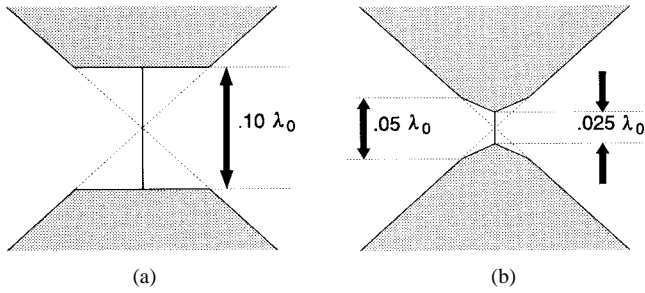


Fig. 4. Closeup of feed regions.

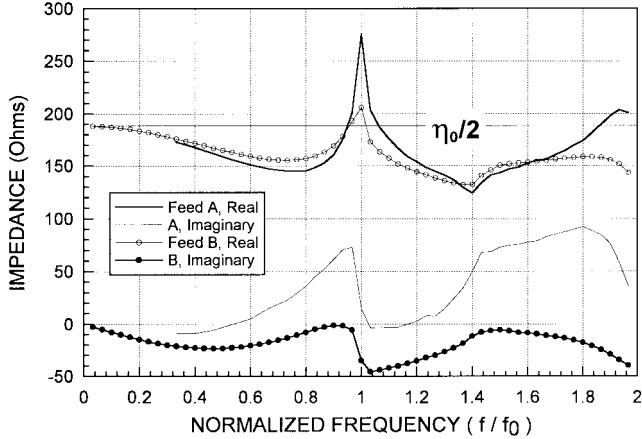


Fig. 5. Planar bicone-array input impedance versus frequency for broadside scan.

feed geometry of Fig. 4(b) provides a better approximation to a point source and, therefore, gives a closer approximation to a self-complementary structure. This is the feed geometry used for all subsequent calculations.

When the planar bicone array is used as a transmitter with sources in phase, for frequencies up to f_0 , it radiates half of its power in each direction normal to the array. Similarly, when receiving, one half the power in a broadside-incidence plane wave will be absorbed by the array when the feed points are loaded by $60\pi \Omega$ impedance. Fig. 6 shows the received, forwardscatter and backscatter power under those conditions of broadside incidence and $\eta_0/2$ load impedance. Within the grating lobe-free region, the received power is very nearly constant, which is a consequence of the frequency-independent self-complementary property. However, as frequency increases through f_0 , the form of the current induced on the bicone plates by the incident wave changes form. The total power scattered in the broadside directions does not change, but the remaining 50% scatters into grating lobes with very little being absorbed. For off-broadside incidence, the received power remains nearly constant at low frequencies, but drops sharply when the first grating lobes become visible at the frequency $f_{GL} = f_0/(1 + \sin \theta_0)$, where θ_0 is the angle of incidence (measured from the $-z$ axis). Thus, although the planar bicone array exhibits frequency-independent input impedance properties, it is only useful up to the grating lobe limiting frequency f_{GL} . Although the input impedance remains acceptably near $\eta_0/2$ above that frequency, most of the radiated power ceases to go into the main beam, instead coupling primarily into the grating lobes.

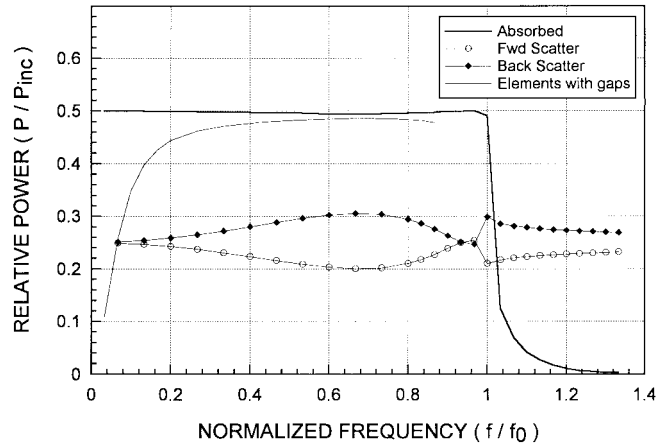


Fig. 6. Received and scattered power, planar bicone array, normal incidence.

Fig. 6 also shows the received power for an array with disconnected [Fig. 3(c)] elements. The air gap between adjacent elements is $\lambda_0/10$ and the feed geometry is the same as in Fig. 4(b). It is clear from this result that as expected from [4] and [6], the interconnection between elements is essential for receiving or radiating low-frequency components of transient waveforms.

IV. TEM HORN ARRAY FREQUENCY RESPONSE

A TEM horn is essentially a pyramidal horn with two sides removed. It is one of the most common antennas used for ultrawide-band transient radiation and reception, but little is known about its properties as an array element. The following presents data for arrays with square lattices, $d_x = d_y = \lambda_0$, and for horns whose interior angle is $\beta = 120^\circ, 60^\circ$, and 35° .

In the low-frequency limit, the input impedance of the TEM horn is not affected by its flare angle. It is purely a function of the unit cell lattice. Hence, for a square lattice, it is still expected that $Z_{in} \approx \eta_0/2$ for $f \ll f_0$. Hence, in computing the array frequency response in the receiving case, a load impedance of $\eta_0/2$ was used. The feed geometry was the same as in Fig. 4(b) when viewed from the $+z$ direction.

Fig. 7 shows the receiving frequency response for the three TEM horns and the planar bicone. As expected, the smaller horn angles provide directionality—on receive, more of the incident power couples into the loads with less being reradiated. However, the frequency response magnitude is less uniform, exhibiting oscillations with increasing frequency. For the transmitting case, by reciprocity the radiated power in the $+z$ direction is the difference between unity and the values in Fig. 7. The peaks in the frequency response magnitude coincide with those frequencies at which the horn length is an integer multiple of one half wavelength.

Fig. 7 indicates that there is an advantage to using TEM horn elements to improve directionality in the frequency range below f_0 . However, their operation must still be restricted to the grating lobe-free range of frequency and scan angle. For an ultrawide-band transmitter, this means that the array lattice spacing must be chosen so that f_0 is equal to or above the highest frequencies that the sources generate. If that condition

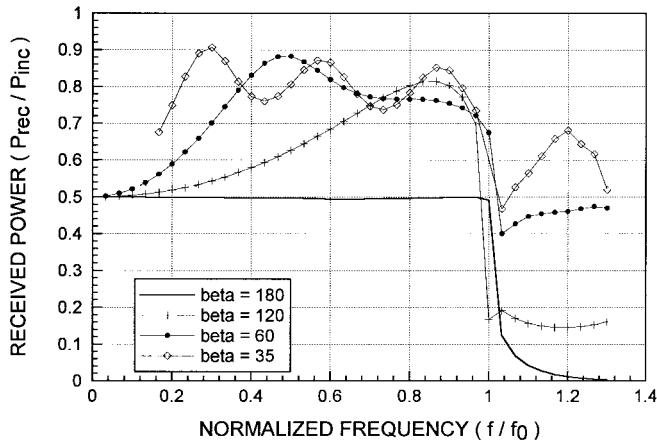


Fig. 7. Received power, normal incidence, planar bicone, and three TEM horn arrays.

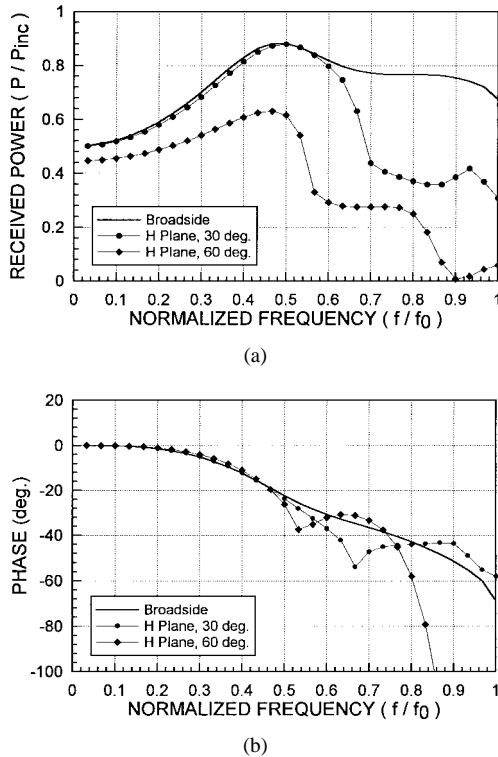


Fig. 8. (a) Received power and (b) phase for $\beta = 60^\circ$ TEM horn array, 0° , 30° and 60° incidence (H plane).

is not met, most of the energy above f_{GL} will not radiate in the intended direction.

Fig. 8 shows the received power and phase for $\beta = 60^\circ$, for scanning to various angles in the H plane. The phase, referenced to the center of the load, is nearly linear up to the grating lobe onset, implying the ability to nondispersively radiate or receive transient waveforms.

V. TEM HORN-ARRAY INPUT IMPEDANCE

The input impedance for an isolated TEM horn may be directly calculated using stereographic and conformal mapping [13]. In the high-frequency limit, this is also the impedance seen by an array element. For the square lattice dimensions,

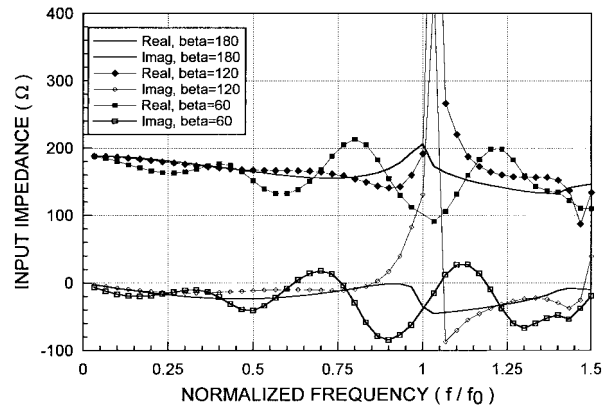


Fig. 9. Input Impedance at broadside scan, planar bicone, and $\beta = 120^\circ$ and $\beta = 60^\circ$ TEM horn arrays.

those limits are $0.493\eta_0$ for $\beta = 120^\circ$, and $0.481\eta_0$ for $\beta = 60^\circ$. In the low-frequency limit, at broadside scan, the array element's input impedance is identical to that of a planar bicone array with the same lattice dimensions $\eta_0/2$. In the intermediate frequency range, however, it is necessary to rely on either calculations or measurements to find Z_{in} .

The feed geometry from Fig. 4(b) is used with the $\beta = 120^\circ$ and $\beta = 60^\circ$ TEM horn elements. The lattice is square with $d_x = d_y = \lambda_0$. Fig. 9 compares Z_{in} versus frequency for the TEM horn elements and the planar bicone element at broadside scan. The oscillations in Z_{in} for the horn elements follow the same pattern as the received power (Fig. 7). As expected, the received power was maximum at those frequencies where Z_{in} is closest to $\eta_0/2$.

Fig. 10 shows the input impedance for four cases with $\beta = 120^\circ$ and $\beta = 60^\circ$ for scanning in the E and H planes. Each graph shows results for scanning to 30° and 60° . Note that the low-frequency limit for input impedance when scanning to the angle θ_0 is $.5\eta_0 \cos(\theta_0)$ or $.5\eta_0 \sec(\theta_0)$ for scanning in the E and H planes, respectively. Both arrays perform better scanning in the E plane. The narrower angle horn is more limited in its scanning ability, having large variations in Z_{in} versus frequency when scanned away from broadside.

In each case in Fig. 10, observe that at the highest frequencies calculated, the input impedance is the same depending only on the flare angle and not on the scan angle or scan plane. This confirms the proposition that the high-frequency limit on Z_{in} depends only on the element's flare angle and aperture dimensions.

VI. CONCLUSIONS

The impedance and scanning properties of TEM horn arrays have been assessed numerically. The limiting case, the planar bicone, was shown to have the frequency-independent property of a self-complementary antenna, making it a useful case for establishing the effects of feed region geometry. Although it radiates bidirectionally, it has the interesting property that its frequency response in the array environment is absolutely flat up to the grating lobe onset limit. A TEM horn array is more unidirectional but, as a consequence, suffers both oscillatory

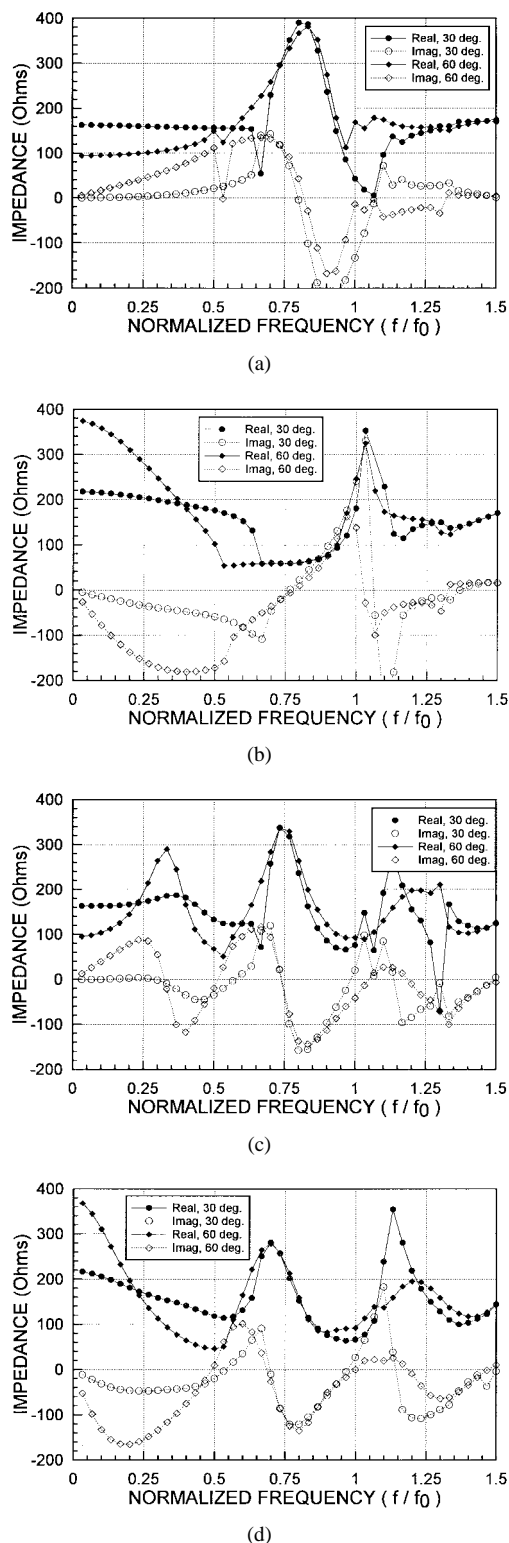


Fig. 10. Input impedance for $\theta = 30^\circ$ and $\beta = 60^\circ$ scan. (a) $\beta = 120^\circ$, E plane. (b) $\beta = 120^\circ$, H plane. (c) $\beta = 60^\circ$, E plane. (d) $\beta = 60^\circ$, H plane.

variations in the input impedance with frequency and increased limits on minimum achievable rise time. Nonetheless, those deficiencies are not severe enough to preclude its use as a time-delay scanned antenna for transient radiation or reception. Finally, elements of both the planar bicone and TEM horn

arrays must be directly connected at the unit cell boundaries to be able to radiate low frequencies.

ACKNOWLEDGMENT

The calculations were performed using resources of the Maui High-Performance Computing Center.

REFERENCES

- [1] C. E. Baum, "From the electromagnetic pulse to high-power electromagnetics," *Proc. IEEE*, vol. 80, pp. 789–817, June 1992.
- [2] L. Carin and S. Vitebsky, "Short-pulse scattering from and the resonances of buried and surface metal mines," *Ultra-Wideband, Short-Pulse Electromagnetics 3*, C. E. Baum, L. Carin, and A.P. Stone, Eds. New York: Plenum, 1997, pp. 499–509.
- [3] D. V. Giri and C. E. Baum, "Temporal and spectral radiation on boresight of a reflector type of impulse radiating antenna (IRA)," *Ultra-Wideband, Short-Pulse Electromagnetics 3*, C. E. Baum, L. Carin, and A.P. Stone, Eds. New York: Plenum, 1997, pp. 65–72.
- [4] C. E. Baum, "Transient arrays," *Ultra-wideband, Short-pulse Electromagnetics 3*, C. E. Baum, L. Carin, and A.P. Stone, Eds. New York: Plenum, 1997, pp. 129–138.
- [5] M. Buttram, "Potential applications in government and industry," *High Power Optically-Activated Solid-State Switches*, A. Rosen and F. Zutavern, Eds. Norwood, MA: Artech House, 1994, ch. 1, p. 25.
- [6] C. E. Baum, "Some characteristics of planar distributed sources for radiating transient pulses," Sensor Simulation Note #100, U.S. Air Force Weapons Lab., Kirtland AFB, NM, Mar. 1970.
- [7] D. T. McGrath and V. Pyati, "Phased-array antenna analysis with the hybrid finite-element method," *IEEE Trans. Antennas Propagat.*, vol. 42, pp. 1625–1630, Dec. 1994.
- [8] —, "Periodic structure analysis using a hybrid finite element method," *Radio Sci.*, vol. 31, pp. 1173–1179, Sept./Oct. 1996.
- [9] T. K. Sarkar, "On the application of the generalized biconjugate gradient method," *J. Electromagn. Waves Applicat.*, vol. 1, pp. 223–242, 1987.
- [10] D. T. McGrath, "Numerical analysis of planar bicone arrays," Sensor Simulation Note No. 403, U.S. Air Force Phillips Lab., Kirtland AFB, NM, Dec. 1996.
- [11] G. A. Deschamps, "Properties of complementary multiterminal planar structures," *IRE Trans. Antennas Propagat.*, vol. AP-7, pp. S371–S378, Dec. 1959.
- [12] N. Inagaki, Y. Isogai, and Y. Mushiaki, "Ichimatsu moyou antenna—Self-complementary antenna with periodic feeding points," *IECE Trans.*, vol. 62, pp. 388–395, 1979.
- [13] F. C. Yang and K. S. H. Lee, "Impedance of a two-conical plate transmission line," Sensor Simulation Note #221, U.S. Air Force Phillips Lab., Kirtland AFB, NM, Nov. 1976.

Daniel T. McGrath (S'82–M'93) received the B.S.E.E. degree from the U.S. Air Force Academy, CO, in 1979, and the M.S.E.E. and Ph.D. degrees from the Air Force Institute of Technology (AFIT), Wright-Patterson AFB, OH, in 1982 and 1993, respectively.

From 1979 to 1982, he worked at the Air Force Armament Laboratory, Eglin AFB, FL, in the area of signal processing and pattern recognition. Following his M.S.E.E. studies, he worked at Rome Air Development Center, Hanscom AFB, MA, from 1983 to 1978, performing experimental validation of novel architectures for phased-array and lens antennas. His dissertation research at AFIT developed computational methods applying waveguide and periodic boundary conditions to the finite-element method for analysis of array antenna mutual coupling. Subsequently, he served from 1993 to 1998 at U.S. Air Force Phillips Laboratory, Kirtland AFB, NM, performing high-power microwave and transient electromagnetics research. In June 1998 he joined Raytheon Systems Company, McKinney, TX.

Carl E. Baum (S'62–M'63–SM'78–F'84), for a photograph and biography, see p. 111 of the January 1999 issue of this TRANSACTIONS.